Am J Cancer Res 2026;16(2):568-577
www.ajcr.us /ISSN:2156-6976/ajcr0169414

Original Article

Comparative study on imaging characteristics of pilocytic astrocytomas in children and adolescents

Yan Gao[1*], Qing Liu[2*], Hailing Liu[1], Honglei Qiu[1], Fengjie Liu[3], Chengkai Cui[4]

[1]Department of Radiology, People's Hospital of Rizhao, Rizhao, Shandong, China; [2]Magnatic Resonance Imaging Room, People's Hospital of Rizhao, Rizhao, Shandong, China; [3]Department of Radiology, Yantai Yuhuangding Hospital, Yantai, Shandong, China; [4]Department of Radiology, Yantai Yantaishan Hospital, Yantai, Shandong, China. [*]Co-first authors.

Received October 19, 2025; Accepted December 11, 2025; Epub February 15, 2026; Published February 28, 2026

Abstract: This study investigated imaging differences of intracranial pilocytic astrocytomas (PA) between children and adolescents. We retrospectively analyzed imaging data from 19 children and 19 adolescents admitted to People's Hospital of Rizhao between January 2018 and December 2024. The mean age was 5.95±2.82 years in the children group and 21.00±3.61 years in the adolescent group. There were no significant differences in sex, extent of resection, tumor extension, or supratentorial/infratentorial location between the two groups. Tumors were significantly larger in the children group compared with the adolescent group (4.39±1.98 cm vs 3.30±0.88, P=0.035). Tumors at midline location were more prevalent in the children group compared with the adolescent group (84.21% vs 31.58%, P=0.001). Significant between-group differences were observed in morphology of regularity (52.63% vs 10.53%, P=0.005), and obstructive hydrocephalus (36.84% vs 5.26%, P=0.017). However, no significant differences were observed between groups in terms of tumor type, enhancement pattern, morphology, edema, or DWI signal. These imaging features, particularly regarding tumor size, midline location, morphological regularity, and obstructive hydrocephalus, may aid in preoperative diagnosis.

Keywords: Pilocytic astrocytomas, children, adolescents, magnetic resonance imaging, computed tomography

Introduction

Intracranial pilocytic astrocytoma (PA) is a slow-growing WHO Grade I tumor classified as a "circumscribed astrocytic gliomas" in the WHO 2021 system [1]. PA accounts for 5-6% of all central nervous system gliomas in the general population, with the proportion increasing to 19.7% in children [2]. Although commonly located in midline structures, the brainstem, and posterior fossa, PA may also involve sites such as the optic tract, periventricular area, and temporal lobes. However, intraventricular involvement is exceedingly rare. PAs are typically slow growing tumors with favorable prognosis, with a reported 20-year survival rate of approximately 79% [3]. However, when located in regions where the contrast enhancement and growth pattern mimic more infiltrative or aggressive lesions, misdiagnosis may occur [4]. Therefore, accurate differential diagnosis of PA is very important.

PA predominantly occurs in children and adolescents. The differentiation of pediatric PA from adolescent PA is clinically important because their treatment and prognoses may differ. However, their accurate differentiation can be challenging for both pathologists and neuroradiologists. Non-invasive imaging methods, such as computerized tomography (CT) and magnetic resonance imaging (MRI), are widely used for PA diagnosis, as they provide both physiological and morphologic information. Particularly, diffusion-weighted imaging (DWI) has become an essential tool in the differential diagnosis of central nervous system tumors. Although previous studies have described radiologic features of PA, most did not differentiate imaging findings between children and adolescents [5]. In addition, only a few studies reported MRI features of PA in children and adolescents, and most were case reports or small series with considerable overlap in conventional imaging features [6, 7]. Due to the rarity of

https://doi.org/10.62347/ARHQ5959

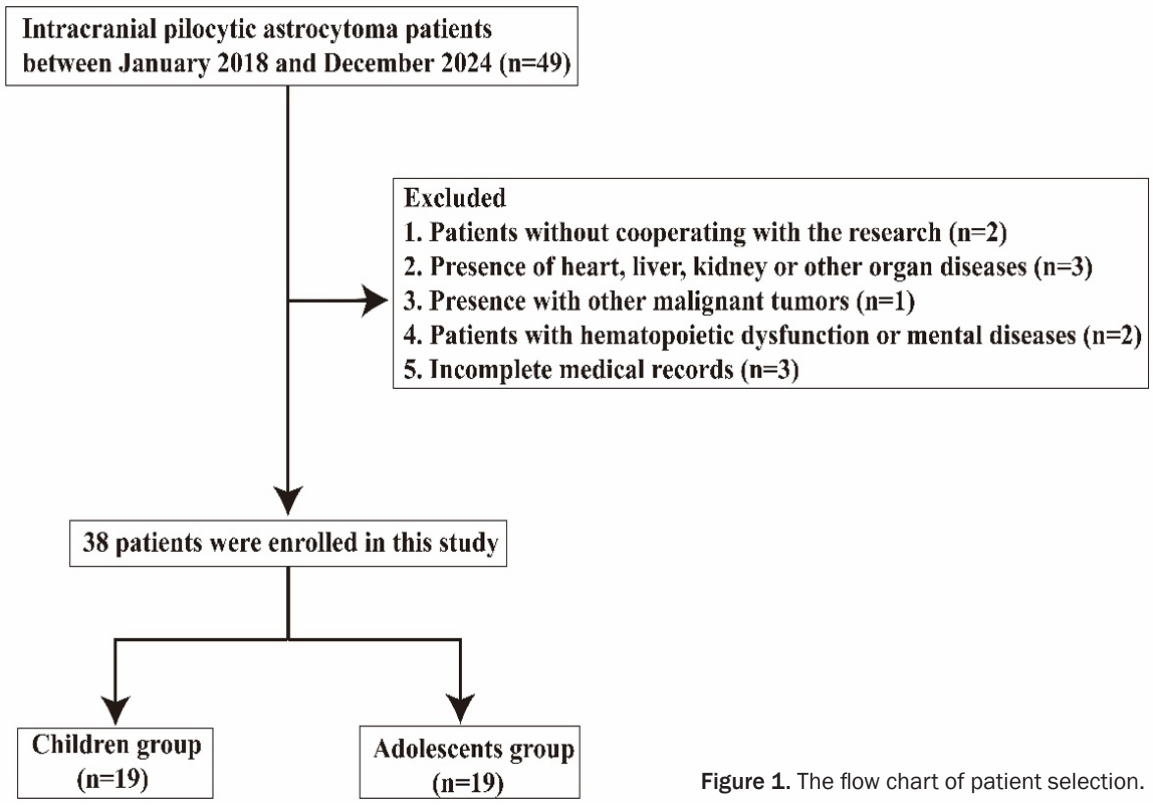

Figure 1. The flow chart of patient selection.

intracranial PA, its age-related differences in locations, imaging features, and other characteristics remains largely unclear. Therefore, the aim of this study was to compare imaging findings and other features of PA between children and adolescents. The results may enhance the diagnostic accuracy and support clinical decision-making and prognostic assessment.

Methods

General information

Between January 2018 and December 2024, a total of 49 AP patients treated in our hospital were initially selected for this retrospective study. According to predefined inclusion and exclusion criteria, 38 AP patients were finally included in this study, including 19 children and 19 adolescents (**Figure 1**). This study was approved by the Ethics Committee of People's Hospital of Rizha (No. 2018-046).

Inclusion criteria: ① Diagnosis of AP based on previously reported criteria [8], confirmed by pathological examination (**Figure 2**); ② No contraindications to the surgery; ③ Regular follow-up after operation; ④ Initial diagnosis; ⑤ No previous radiotherapy or chemotherapy; ⑥ Availability of head MRI and CT imaging data; ⑦ Complete medical records. Exclusion criteria: ① Presence of heart, liver, kidney or other organ diseases; ② Presence with other malignant tumors, hematopoietic dysfunction, or mental diseases.

Data collection

Clinical data of all patients were collected from electronic medical records, including age, gender, extent of resection, tumor extension, tumor location, tumor size, tumor morphology, tumor type, enhancement pattern, obstructive hydrocephalus, edema, signal intensity of diffusion weighted imaging (DWI), and calcification.

Outcomes measures

MRI scanning: MRI was conducted using GE Signal 1.5T and Siemens Verio 3.0T superconducting scanners. A head coil was used for all scanning. Conventional MRI comprised SE and FSE sequences: SE-T1WI (TR 500 ms, TE 30 ms) and FSE-T2WI (TR 3000 ms, TE 100 ms).

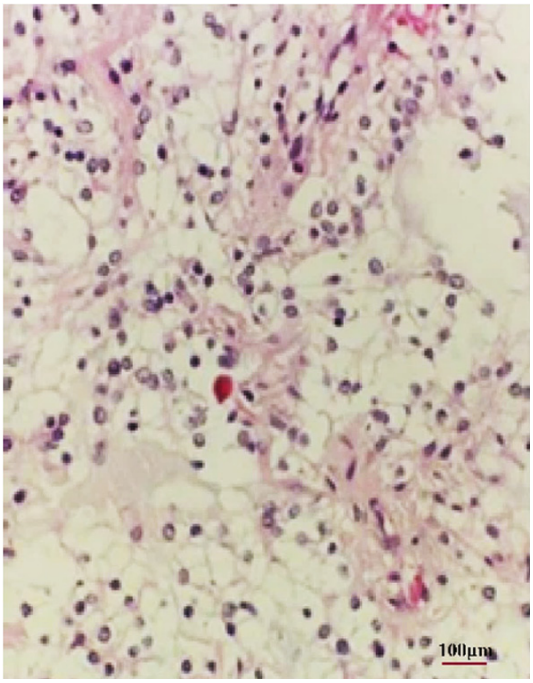

Figure 2. Pathological findings of PA (HE, ×200). Microscopically, the tumor demonstrated alternating dense and loose areas with perinuclear halos. Eosinophilic granular bodies and Rosenthal fibers are visible. Note: PA, Pilocytic astrocytomas; HE, Hematoxylin-Eosin.

Images were acquired in transverse, sagittal, and coronal planes. The field of view (FOV) was 24×24 cm^2, matrix was 128×128, and slice thickness was 10 mm. For DWI scanning, b-values were set at 0 (low) and 1000 s/mm^2 (high). Contrast-enhanced scanning employed the Gadopentetate Dimeglumine (Gd-DTPA) and Gadotericate Dimeglumine (Gd-DOTA) at 0.2 ml/kg, administered at a flow rate of 2 ml/s.

CT scanning: CT scans were conducted using either a Siemens Somatom Definition Flash CT scanner or a Philips Ingenuity CT scanner. The tube voltage was 120 kV and the tube current was 270 mAs. The parameters were as follows: scanning speed: 1 revolution per second; slice thickness: 5 mm and 1 mm; interval 5 ms; matrix: 512×512.

Image analysis: All imaging data were independently reviewed by two senior attending radiologists. All images were evaluated in a blinded manner. In cases of disagreement, a senior radiologist was consulted to reach a consensus diagnosis.

Statistical analysis

Data analysis was conducted using SPSS 22.0. Continuous variables were expressed as Mean ± Standard deviation (SD), and the comparison between two groups was performed using independent t test. Categorical variables were presented as frequencies and percentages (%), and the comparison between two groups was performed using χ^2 test. Fisher test was conducted if total sample size was less than 40. A *P*-value <0.05 was considered statistically significant.

Results

Comparison of general information

As shown in **Table 1**, there were no obvious differences in terms of gender, extent of resection, or tumor extension between the two groups (all P>0.05). In terms of the tumor location, there were 14 supratentorial cases (73.7%) in children group and 10 cases (52.6%) in the adolescents group; whereas there were 5 infratentorial cases (26.3%) in children group and 9 cases (47.4%) in adolescent group (P=0.178).

The midline regions of saddle area, basal ganglia-thalamic region, ventricles and cerebellar vermis were defined as midline regions, while the sites outside the midline regions in cerebral hemispheres and cerebellar hemispheres were defined as non-midline regions. PA in the children group predominantly occurred in midline regions, while PA in the adolescent group mainly occurred in non-midline regions, with a significant difference between the two groups (P<0.05).

Comparison of tumor diameter, morphology, and obstructive hydrocephalus

As shown in **Table 2**, the mean tumor diameter in the children group (4.39±1.98 cm) was significantly larger than that in the adolescent group (3.30±0.88 cm) (P<0.05). In the children group, 10 cases (52.6%) exhibited regular morphology such as round or sub-round, compared with 2 cases (10.5%) in the adolescent group (P<0.05). As shown in **Figure 3**, obstructive hydrocephalus occurred in 7 children (36.8%) and 1 adolescent (5.3%) (P<0.05).

Table 1. Comparison of general information between children group and adolescent group

Parameters	Children group (N=19)	Adolescents group (N=19)	t/χ^2 value	*P* value
Age (Years)	5.95±2.82	21.00±3.61	14.320	<0.001
Gender			-	0.508
Male	13	10		
Female	6	9		
Extend of resection			1.581	0.664
Gross total resection	10	11		
Subtotal resection	4	2		
Partial resection	3	2		
Biopsy	2	4		
Tumor Extension			0.364	0.834
Local	16	17		
Regional	2	1		
Distal	1	1		
Tumor Location				
Supratentoria	14	10		0.313
Infratentoria	5	9		
Midline site	16	6		0.003
Deviation from midline site	3	13		
Size of tumor (cm)	4.39±1.98	3.30±0.88	2.193	0.035

Table 2. Comparison of imaging characteristics of pilocytic astrocytomas between children group and adolescent group

Parameters	Children group (N=19)	Adolescents group (N=19)	t/χ^2 value	*P* value
Morphology				0.013
Regularity	10	2		
Irregularity	9	17		
Type			0.643	0.725
Cystic	1	1		
Cystic-solid	13	15		
Solid	5	3		
The enhancing patterns				>0.999
Marked enhancement	18	17		
Mild enhancement	1	2		
Obstructive hydrocephalus				0.042
Yes	7	1		
No	12	18		
Edema				0.604
No and mild edema	18	16		
Moderate and severe edema	1	3		
DWI				0.487
Low intensity signal	19	17		
Isointense to slightly hyperintense signal	0	2		
Calcification				0.180
Yes	14	18		
No	5	1		

DWI: diffusion-weighted imaging.

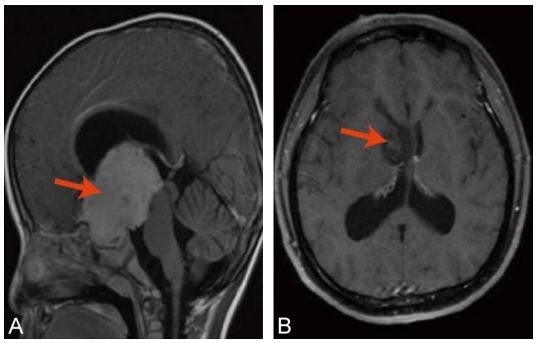

Figure 3. Obstructive hydrocephalus detected by MRI scanning. A. Female, 3 years old, MRI image of saddle PA, with obstructive hydrocephalus. B. Female, 23 years old, MRI images of solid PA in the right basal ganglia area, without obstructive hydrocephalus. The red arrow indicates PA. Note: MRI, Magnetic resonance imaging; PA, Pilocytic astrocytomas.

Comparison of tumor classification

Based on imaging characteristics of PA shown in **Figure 4**, tumors were classified into three types: ① Cystic type: No significant solid components were observed, with or without cyst wall enhancement; ② Cystic-solid type: Coexistence of solid components and cystic components of varying proportions. Moreover, solid components exhibited variable enhancement patterns, predominantly showing marked heterogeneous enhancement, while cystic areas showed no enhancement. This subtype was further subdivided into mixed cystic-solid type and cystic lesions with mural nodule; ③ Solid type: No discernible cystic components were observed, with uniform or heterogeneous enhancement.

In the children group, there were 1 cystic case (5.3%), 13 cystic-solid cases (68.4%) comprising 4 cystic plus with mural nodule and 9 mixed cystic-solid, and 5 solid cases (26.3%); while in the adolescent group, there were 1 cystic case (5.3%), 15 cystic-solid cases (78.9%) comprising 3 cyst-with-nodule and 12 mixed cystic-solid types, and 5 solid cases (15.8%). No significant difference were detected between the two groups (P>0.05).

Comparison of image enhancement, DWI signal, and peritumoral oedema

As shown in **Figure 5**, mild tumor enhancement was observed in 1 case (5.3%) in the children group and 2 cases (10.5%) in the adolescent group, and all other cases exhibited marked tumor enhancement. All tumors in the children group displayed low DWI signal intensity, while 2 adolescent cases (10.5%) showed isointense to slightly hyperintense signals, with others presenting low signal intensity. Peritumoral oedema was observed in 1 case (5.3%) in the children group and 3 cases (15.8%) in the adolescent group, all presenting moderate to severe oedema; the remaining cases exhibited mild or no oedema. None of these differences were statistically significant between groups (P>0.05).

Comparison of calcification

As shown in **Figure 6**, calcifications appeared as punctate, patchy, or shell-like shape. Calcification was observed in 14 out of 19 cases (73.7%) in the children group, which was comparable to 18 out of 19 cases (94.7%) in the adolescent group (P>0.05).

Discussion

Gliomas originate from neuroepithelial tissue and represent a clinically prevalent intracranial tumor, often exhibiting cystic degeneration and necrosis [9]. The most prevalent subtype of glioma is astrocytoma, a common pediatric brain tumor. Pathologically, astrocytomas are classified into four grades: Grade I and II astrocytomas exhibit well-differentiated features and are considered benign or borderline malignant, whereas Grade III and IV astrocytomas are malignant, characterized by diffuse infiltrative growth with indistinct margins. In 1937, Penfield designated this tumor pilocytic astrocytoma (PA) based on the fine, hair-like glial fibers projecting from both ends of the tumor cells [10]. PA accounts for approximately 4.0%-5.0% of intracranial gliomas and is classified as Grade I astrocytoma. PA is a well-defined, slow-growing astrocytoma with a favorable prognosis, predominantly affecting children and adolescents, occasionally in adults, with a slightly higher incidence in males [11].

This retrospective analysis identified two incidence peaks at 0-10 years and 15-25 years, consistent with previous literature indicating a predilection for childhood and adolescence [12]. PA frequently arises near the intracranial midline, including regions such as the cerebellum, optic nerves, and hypothalamus, whilst

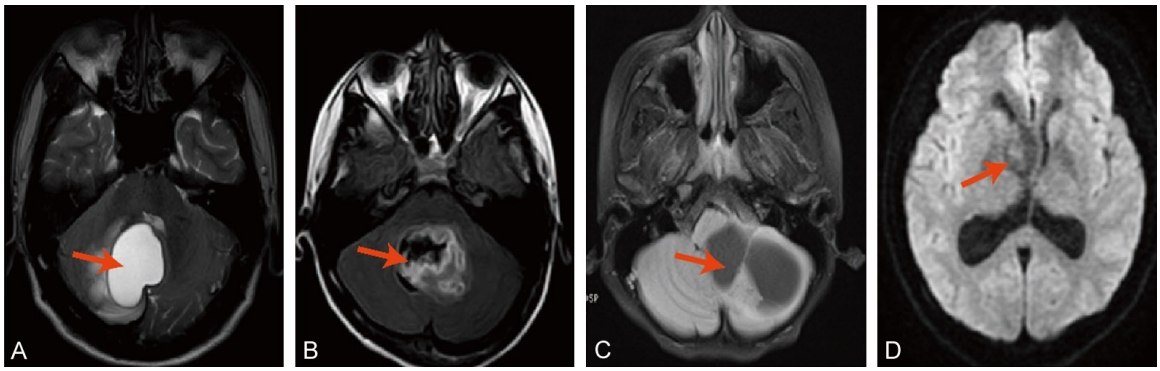

Figure 4. Tumor classification detected by MRI scanning. A. Female, 15 years old, MRI images of cystic right cerebellar hemisphere PA, with cystic type. B. Female, 10 years old, MRI image of mixed cystic solid PA in cerebellar vermis. C. Male, 15 years old, MRI images of left cerebellar hemisphere cyst-with-nodule PA. D. Female, 22 years old, MRI images of solid PA in the right basal ganglia area. The red arrow indicates PA. Note: PA, Pilocytic astrocytomas; MRI, Magnetic resonance imaging.

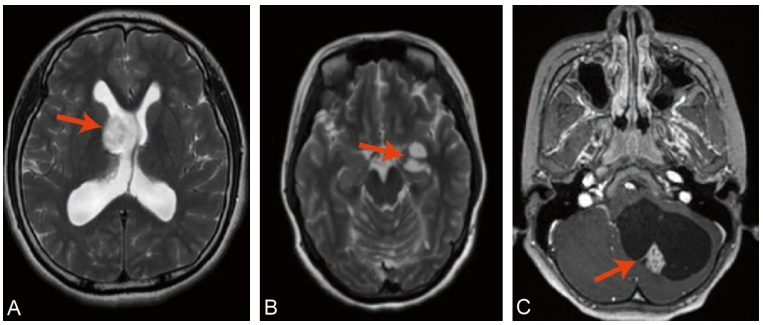

Figure 5. Image enhancement, DWI Signal, and peritumoral oedema in PA. A. The lesion appeared as a solid mass with regular contours, exhibiting heterogeneous T2 signal intensity. The slightly hyperintense T2-weighted region demonstrated isointense to slightly hyperintense DWI signal with marked enhancement. The extremely hyperintense T2-weighted region showed hypointense signal on DWI with minimal enhancement. No perilesional oedema was observed. B. The lesion exhibited an irregular shape with long T1 and long T2 signal intensity resembling cerebrospinal fluid, demonstrating uniform signal intensity. Mild peripheral enhancement was observed without surrounding oedema. C. The nodular component exhibited isointense T2 signal, with no enhancement of the cyst wall. The solid nodular component demonstrated marked, woolly-ball-like nodular enhancement. The red arrow indicates PA. Note: DWI, Diffusion weighted imaging; PA, Pilocytic astrocytomas.

less common sites include cerebral hemispheres, ventricles, and the spinal cord [13]. Previous reports indicating a higher incidence of subparietal lesions than supratentorial lesions in children are inconsistent with the present findings, potentially due to insufficient case numbers or non-single-center case collection. The prevalence of supratentorial lesions in individuals over 20 years old [14], particularly in cerebral lobes [15], is consistent with this study. Diagnosis of PA is based on the identification of Rosenthal fibers, characterized microscopically by a mixture of hair-like astrocytes and sparse mature glial fibres [16].

Currently, CT and MRI are widely used and highly valuable imaging modalities in clinical practice [17, 18]. With advances in medical imaging technology, the precision of CT, MRI and other techniques has improved markedly, substantially improving the diagnosis of malignant tumors [19]. Owing to the rich vascularity of PA, the solid components-including wall nodules and cyst walls-typically exhibited uniform or heterogeneous enhancement. In some tumors, only solid elements such as mural nodules enhance, whilst cyst walls show minimal or no enhancement; certain cystic cases may demonstrate no enhancement at all. The pathological basis for this enhancement differs from most other tumors. Generally, enhancement intensity in brain tumors correlates positively with malignancy: higher malignancy correlates with more immature tumor vasculature and greater disruption of the blood-brain barrier. However, studies have shown the presence of contrast-filled endocytic vesicles within vascular cells of PA following contrast administration [20]. This demonstrates that contrast enhancement in PA arises from

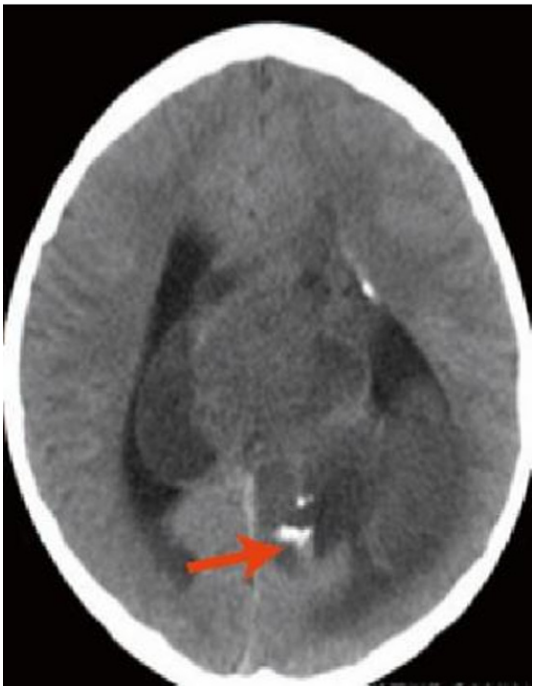

Figure 6. CT image of intraventricular PA showing mixed cystic-solid lesions with heterogeneous low density, multiple patchy calcifications around the periphery, and obstructive hydrocephalus of the ventricular system. Note: PA, Pilocytic astrocytomas; CT, Computerized tomography.

increased capillary permeability rather than blood-brain barrier disruption.

Non-enhanced cyst walls on contrast-enhanced imaging are considered pseudocysts, likely composed of reactive glial proliferation or compressed brain tissue. In contrast, enhanced cyst walls mimic histological features of solid components and wall nodules, comprising active tumor cells and proliferative neovasculature. Previous studies have reported that CT values in PA correlate with vascular permeability, exhibiting characteristic imaging features such as cystic wall nodules or solid masses [21]; histopathological findings also varied significantly among PA subtypes [22], supporting that imaging could provide valuable guidance for surgical planning. CT provides high-resolution cross-sectional images that clearly delineate lesion size, location, and morphology, thereby holding significant diagnostic value for tumor assessment [23]. Due to the high protein content of PA cyst, plain CT scans typically reveal low-density cystic areas, while solid components appear isodense or slightly hypodense. Calcification occurs in approximately 11% of PAs and presents hyperdense on plain CT scans [24]. The scattered hyperdense calcifications on CT scans observed in this study align with previous research reports [25]. Overall, CT generally serves only as a screening tool for detecting finer calcifications that are challenging for MRI, yet its plain scan features provide limited discriminatory advantages.

MRI is a more clinically valuable imaging modality than CT, capable of producing cross-sectional, coronal, and sagittal views simultaneously. MRI scanning provides the clearer visualization of tumors and surrounding structures, thereby enhancing diagnostic accuracy. Some studies suggested that characteristic MRI features of PA could potentially enhance preoperative diagnostic accuracy [26, 27]. Further studies indicated that CT demonstrates lower specificity and accuracy than MRI in diagnosing PA, with statistically significant differences. MRI consistently reveals characteristic features aligned with PA pathology, including lesion morphology, signal characteristics, and enhancement patterns. In MRI imaging, the degree of enhancement in gliomas typically correlate positively with malignancy, as higher grade exhibit immature vascular development and greater blood-brain barrier disruption, resulting in marked enhancement. The pronounced enhancement typically seen in PAs may be attributed to porous endothelium of neovascularisation and hyaline change of proliferating microvascular walls, both of which facilitate contrast extravasation. Typical enhancement patterns of PA include: ① Extremely long T2 with marked enhancement, reflecting loose tissue structure, high water content, and vascular hyperpermeability. This feature is typically seen in PA and chordoid glioma; the latter is generally confined to specific sites and exhibit relatively lower signal intensity than PA on non-contrast scans [28]. ② Ground-glass or “woolly-woolly” enhancement, resembling high-grade gliomas but with low DWI signal intensity, which is believed to result from gadolinium leakage secondary to necrosis-related inflammation or vascular hyperpermeability. This imaging feature, termed “the cut green pepper sign” [29], has gained widespread recognition among radiologists. ③ Non-enhancement or minimal enhancement, occurred when tumors possessed well-developed vasculature and a relatively

intact blood-brain barrier [30]. The two cases of minimal enhancement in this study fell into this category.

PA are typically associated with absent or mild oedema, further supporting their benign nature. Moreover, cystic-solid tumors predominate in PA classification. In this study, 28 cases (74%) were cystic-solid, consistent with previous literature [31]. Except for T2 penetration effects [32], higher DWI signal intensity in intracranial tumors generally correlates with increased malignancy [33]. In this study, 36 PA lesions exhibited low DWI signal intensity, with only two exhibiting isointense to slightly hyperintense signals, further confirming the benign nature of PA. Previous literature has reported that PAs predominantly exhibit high enhancement and perfusion [16]. However, other studies have indicated that despite marked enhancement, most PAs show minimal microvascular proliferation and slow blood flow, typically presenting as low perfusion [34]. Further MRI perfusion studies are warranted to clarify these discrepancies.

In clinical practice, intracranial PAs should be cautiously differentiated from several other intracranial lesions, with particular attention to age of onset, tumor location, and imaging characteristics. For example: ① Other-grade gliomas: Grade II diffuse astrocytomas typically demonstrate indistinct margins with absent or weak enhancement. As tumor grade increase, enhancement becomes more pronounced, cystic necrosis becomes more prevalent, and DWI signal intensity gradually increases. High-grade gliomas are more common in the elderly [35]. Oligodendrogliomas predominantly occurs in the frontal lobe and characteristically exhibit band-like calcifications [36]. Ependymomas rarely exhibit ground-glass/woolly enhancement; they are closely associated with lateral ventricle walls and may mold to the shape of the fourth ventricle when located there [37]. ② Solitary metastatic lesions: Metastases commonly involve the grey-white matter junction within the cerebral hemispheres, tend to deviate from midline structures, and are often accompanied by significant oedema. They are more prevalent in the elderlies and can be easily distinguished if a primary malignancy is known. ③ Sellar region tumors: The differentiation from craniopharyngioma and pituitary adenoma is essential. Craniopharyngioma frequently exhibit shell-like calcification, while pituitary adenomas are associated with loss of normal adenohypophyseal signal and frequently manifest endocrine disturbances [38]. Sella PA predominantly occurs in infants and is referred to as 'infantile-type' PA, indicating its younger age of onset [39]. ④ Haemangioblastoma: The classic diagnostic triad of haemangioblastoma includes peritumoral oedema, hyperenhancement with increased perfusion of the nodular components, and prominent flow voids [40].

Conclusion

Intracranial PAs exhibit two peak incidence periods: 0-10 years and 15-25 years with differences in lesion location, obstructive hydrocephalus, tumor size, and morphology between the two age groups. PAs typically present marked heterogeneous enhancement, low DWI signal, mild or absent peritumoral oedema, a predominantly cystic-solid composition, and frequent calcifications, making diagnosis generally straightforward. When differentiation remained difficult, surgical pathology was required for definitive confirmation.

However, there are some shortcomings of this study, including single-center study with a small sample size, lack of long-term follow-up data, absence of subgroup comparison, and no investigation of underlying mechanism. Future multicenter studies with larger sample size and extended follow-up are needed to further confirm these findings.

Disclosure of conflict of interest

None.

Address correspondence to: Chengkai Cui, Department of Imaging, Yantai Yantaishan Hospital, No. 10087, Keji Avenue, Laishan District, Yantai 264000, Shandong, China. Tel: +86-0535-6863159; Fax: +86-0535-6863159; E-mail: ytscck@163.com

References

[1] Castillo M, Scatliff JH, Bouldin TW and Suzuki K. Radiologic-pathologic correlation: intracranial astrocytoma. AJNR Am J Neuroradiol 1992; 13: 1609-1616.

[2] Korkmazer B, Arslan S, Onal EM, Ozogul M, Urganci N, Isler C, Comunoglu N, Kizilkilic O, Kocer N and Islak C. Imaging findings of intraventricular pilocytic astrocytoma. Br J Radiol 2023; 96: 20220598.
[3] Park YW, Kim D, Eom J, Ahn SS, Moon JH, Kim EH, Kang SG, Chang JH, Kim SH and Lee SK. A diagnostic tree for differentiation of adult pilocytic astrocytomas from high-grade gliomas. Eur J Radiol 2021; 143: 109946.
[4] Ishida Y, Tsuda M, Sawamura Y, Fujii K, Murai H, Horiuchi N, Orba Y, Sawa H, Hall WW, Nagashima K and Tanaka S. "Integrated diagnosis" of pilocytic astrocytoma: Molecular diagnostic procedure for an unusual case. Pathol Int 2018; 68: 694-699.
[5] Reis GF and Tihan T. Practical molecular pathologic diagnosis of pilocytic astrocytomas. Surg Pathol Clin 2015; 8: 63-71.
[6] Zhou X, Su Y, Huang W, Lin X, Xing Z and Cao D. Differentiation between supratentorial pilocytic astrocytoma and extraventricular ependymoma using multiparametric MRI. Acta Radiol 2022; 63: 1661-1668.
[7] Gaudino S, Martucci M, Russo R, Visconti E, Gangemi E, D'Argento F, Verdolotti T, Lauriola L and Colosimo C. MR imaging of brain pilocytic astrocytoma: beyond the stereotype of benign astrocytoma. Childs Nerv Syst 2017; 33: 35-54.
[8] Vats N, Sengupta A, Gupta RK, Patir R, Vaishya S, Ahlawat S, Saini J, Agarwal S and Singh A. Differentiation of pilocytic astrocytoma from glioblastoma using a machine-learning framework based upon quantitative T1 perfusion MRI. Magn Reson Imaging 2023; 98: 76-82.
[9] Galbraith K and Snuderl M. Molecular pathology of gliomas. Clin Lab Med 2024; 44: 149-159.
[10] Knight J, Karsonovich T and De Jesus O. Pilocytic astrocytoma. In: editors. StatPearls. Treasure Island (FL): 2025.
[11] Shin I, Park YW, Ahn SS, Kim J, Chang JH, Kim SH and Lee SK. Clinical factors and conventional MRI may independently predict progression-free survival and overall survival in adult pilocytic astrocytomas. Neuroradiology 2022; 64: 1529-1537.
[12] Parsons MW, Whipple NS, Poppe MM, Mendez JS, Cannon DM and Burt LM. The use and efficacy of chemotherapy and radiotherapy in children and adults with pilocytic astrocytoma. J Neurooncol 2021; 151: 93-101.
[13] Ostrom QT, Kruchko C and Barnholtz-Sloan JS. Pilocytic astrocytomas: where do they belong in cancer reporting? Neuro Oncol 2020; 22: 298-300.
[14] Reis GF, Bloomer MM, Perry A, Phillips JJ, Grenert JP, Karnezis AN and Tihan T. Pilocytic astrocytomas of the optic nerve and their relation to pilocytic astrocytomas elsewhere in the central nervous system. Mod Pathol 2013; 26: 1279-1287.
[15] Kristiansen I, Eklund C, Strinnholm M, Stromberg B, Tornhage M and Frisk P. Cognitive, language, and school performance in children and young adults treated for low-grade astrocytoma in the posterior fossa in childhood. Cancer Rep (Hoboken) 2022; 5: e1494.
[16] de Fatima Vasco Aragao M, Law M, Batista de Almeida D, Fatterpekar G, Delman B, Bader AS, Pelaez M, Fowkes M, Vieira de Mello R and Moraes Valenca M. Comparison of perfusion, diffusion, and MR spectroscopy between low-grade enhancing pilocytic astrocytomas and high-grade astrocytomas. AJNR Am J Neuroradiol 2014; 35: 1495-1502.
[17] Kitamura N, Hasebe T, Kasai R, Kasuya S, Nakatsuka T, Kudo H, Higuchi M, Nakano K, Hiruta N, Kameda N, Ogata K, Watanabe Y, Morita H and Terada H. Pilocytic astrocytomas in elderly adults. Neuroradiol J 2010; 23: 690-695.
[18] Alkonyi B, Nowak J, Gnekow AK, Pietsch T and Warmuth-Metz M. Differential imaging characteristics and dissemination potential of pilomyxoid astrocytomas versus pilocytic astrocytomas. Neuroradiology 2015; 57: 625-638.
[19] Alnawafleh TM, Radzi Y, Alshipli M, Oglat AA and Alflahat A. A comprehensive review of the recent advancements in imaging segmentation and registration techniques for glioblastoma and focusing on the utilization of magnetic resonance imaging (MRI) and computed tomography (CT) scans. Curr Med Imaging 2024; 20: e15734056309829.
[20] Takeuchi H, Kubota T, Sato K and Arishima H. Ultrastructure of capillary endothelium in pilocytic astrocytomas. Brain Tumor Pathol 2004; 21: 23-26.
[21] Agrawal I, Bano S, Chaudhary A and Ahuja A. Role of permeability surface area product in grading of brain gliomas using CT perfusion. Asian J Neurosurg 2023; 18: 751-760.
[22] Parsa CF and Givrad S. Pilocytic astrocytomas as hamartomas: implications for treatment. Br J Ophthalmol 2008; 92: 3-6.
[23] Tans JT and de Jongh IE. Computed tomography of supratentorial astrocytoma. Clin Neurol Neurosurg 1978; 80: 156-168.
[24] Hernandez-Resendiz R, Villanueva-Castro E, Mateo-Nouel EJ, Gomez-Apo E, Penafiel-Salgado C, Salinas-Lara C and Tena-Suck ML. Calcified pilocytic astrocytomas and calcifying pseudoneoplasms of the neuraxis: a diagnostic challenge. Cureus 2024; 16: e51765.
[25] Xia J, Yin B, Liu L, Lu Y, Geng D and Tian W. Imaging features of pilocytic astrocytoma in cerebral ventricles. Clin Neuroradiol 2016; 26: 341-346.

[26] Grand SD, Kremer S, Tropres IM, Hoffmann DM, Chabardes SJ, Lefournier V, Berger FR, Pasteris C, Krainik A, Pasquier BM, Peoch M and Le Bas JF. Perfusion-sensitive MRI of pilocytic astrocytomas: initial results. Neuroradiology 2007; 49: 545-550.
[27] Coakley KJ, Huston J 3rd, Scheithauer BW, Forbes G and Kelly PJ. Pilocytic astrocytomas: well-demarcated magnetic resonance appearance despite frequent infiltration histologically. Mayo Clin Proc 1995; 70: 747-751.
[28] Wang J, Liu Z, Du J, Cui Y, Fang J, Xu L and Li G. The clinicopathological features of pituicytoma and the differential diagnosis of sellar glioma. Neuropathology 2016; 36: 432-440.
[29] Xu S, Yang W, Luo Y, Wang X, Li Y, Meng X, Zhang Y, Zeng H and Huang B. A novel MRI feature, the cut green pepper sign, can help differentiate a suprasellar pilocytic astrocytoma from an adamantinomatous craniopharyngioma. BMC Med Imaging 2023; 23: 191.
[30] Mao Y, Kong X, Luo Y, Xi F, Li Y and Ma J. A fusion model of MRI deep transfer learning and radiomics for discriminating between pilocytic astrocytoma and adamantinomatous craniopharyngioma. Acad Radiol 2025; 32: 2197-2208.
[31] Xu H, Niu HL, Wang FH, Xu XK, Wang W, Yuan L, Chen K, Gao Q, Li LP, Xia JQ and Guo ZM. Clinicopathological and molecular characteristics of pediatric gliomas: analysis of 111 cases. Zhonghua Bing Li Xue Za Zhi 2024; 53: 922-928.
[32] Bale TA and Rosenblum MK. The 2021 WHO classification of tumors of the central nervous system: an update on pediatric low-grade gliomas and glioneuronal tumors. Brain Pathol 2022; 32: e13060.
[33] Kim M, Jung SY, Park JE, Jo Y, Park SY, Nam SJ, Kim JH and Kim HS. Diffusion- and perfusion-weighted MRI radiomics model may predict isocitrate dehydrogenase (IDH) mutation and tumor aggressiveness in diffuse lower grade glioma. Eur Radiol 2020; 30: 2142-2151.
[34] Wang XC, Zhang H, Tan Y, Qin JB, Wu XF, Wang L and Zhang L. Combined value of susceptibility-weighted and perfusion-weighted imaging in assessing who grade for brain astrocytomas. J Magn Reson Imaging 2014; 39: 1569-1574.
[35] Klein R and Roggendorf W. Increased microglia proliferation separates pilocytic astrocytomas from diffuse astrocytomas: a double labeling study. Acta Neuropathol 2001; 101: 245-248.
[36] Tork CA, Hall WA and Atkinson C. Oligodendroglioma. In: editors. StatPearls. Treasure Island (FL): 2025.
[37] Bertero L, Ricci AA, Tampieri C, Cassoni P and Modena P. Ependymomas. Pathologica 2022; 114: 436-446.
[38] Schwetye KE and Dahiya SM. Sellar tumors. Surg Pathol Clin 2020; 13: 305-329.
[39] Tauziede-Espariat A, Beccaria K, Dangouloff-Ros V, Sievers P, Meurgey A, Pissaloux D, Appay R, Saffroy R, Grill J, Mariet C, Bourdeaut F, Hasty L, Metais A, Chretien F, Blauwblomme T, Puget S, Boddaert N and Varlet P; RENOCLIP LOC. A comprehensive analysis of infantile central nervous system tumors to improve distinctive criteria for infant-type hemispheric glioma versus desmoplastic infantile ganglioglioma/astrocytoma. Brain Pathol 2023; 33: e13182.
[40] Khan MM, Hall WA and Belkhair S. Hemangioblastoma. In: editors. StatPearls. Treasure Island (FL): 2025.